Journal of proteome research

pubs.acs.org/jpr

Article

Multiomics Evaluation of Human iPSCs and iPSC-Derived Neurons

Gwang Bin Lee,[#] Wan Nur Atiqah binti Mazli,[#] and Ling Hao*

Cite This: https://doi.org/10.1021/acs.jproteome.3c00790

Read Online

ACCESS | Metrics & More | Article Recommendations | Supporting Information

ABSTRACT: Human induced pluripotent stem cells (iPSCs) can be differentiated into neurons, providing living human neurons to model brain diseases. However, it is unclear how different types of molecules work together to regulate stem cell and neuron biology in healthy and disease states. In this study, we conducted integrated proteomics, lipidomics, and metabolomics analyses with confident identification, accurate quantification, and reproducible measurements to compare the molecular profiles of human iPSCs and iPSC-derived neurons. Proteins, lipids, and metabolites related to mitosis, DNA replication, pluripotency, glycosphingolipids, and energy metabolism were highly enriched in iPSCs, whereas synaptic proteins, neurotransmitters, polyunsaturated fatty acids, cardiolipins, and axon guidance pathways were highly enriched in neurons. Mutations in the *GRN* gene lead to the deficiency of the progranulin (PGRN) protein, which has been associated with various neurodegenerative diseases. Using this multiomics platform, we evaluated the impact of PGRN deficiency on iPSCs and neurons at the whole-cell level. Proteomics, lipidomics, and metabolomics analyses implicated PGRN's roles in neuroinflammation, purine metabolism, and neurite outgrowth, revealing commonly altered pathways related to neuron projection, synaptic dysfunction, and brain metabolism. Multiomics data sets also pointed toward the same hypothesis that neurons seem to be more susceptible to PGRN loss compared to iPSCs, consistent with the neurological symptoms and cognitive impairment from patients carrying inherited *GRN* mutations.

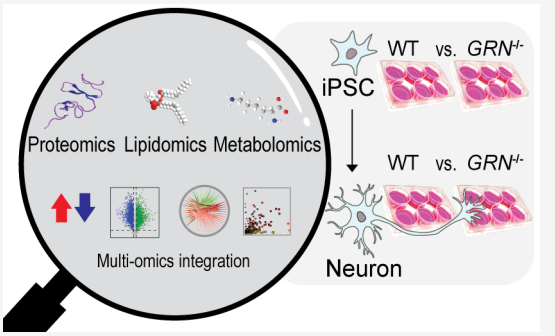

KEYWORDS: *multiomics, proteomics, lipidomics, metabolomics, iPSC, neuron, iPSC-derived neuron, neuron differentiation, GRN, progranulin*

INTRODUCTION

Human induced pluripotent stem cells (iPSCs), derived from somatic cells, are reprogrammed embryonic-like pluripotent cells to enable unlimited development.[1] Human iPSCs can be differentiated into different cell types to model various human diseases.[1] Particularly, iPSC-derived neurons allow researchers to access living human neurons to model brain diseases.[2,3] Various omics studies have been conducted in iPSCs or neurons, such as genomics, transcriptomics, proteomics, metabolomics, and lipidomics.[4−7] However, it is still unclear how different types of molecules work together to govern stem cell and neuron biology as well as neuron differentiation. There is also no report that directly compares molecular profiles between iPSCs and neurons using an integrated proteomics, lipidomics, and metabolomics platform.

Multiomics analysis has been used to unravel the complex biological processes underlying neurodegenerative diseases.[6,8,9] Multiomics experiments must be paired with sophisticated bioinformatic tools to decipher the large-scale multidimensional data sets and integrate different omics data sets into the same biological processes, where genes control protein expression and proteins serve as enzymes for lipid and metabolic pathways.[10−13] Network-based multiomics integration perceives biological systems as interconnected units, where each omics layer contributes to uncovering the authentic connections within the networks.[14] Enabled by these bioinformatics tools, integrating proteomics, lipidomics, and metabolomics analyses of iPSCs and neurons can provide us a holistic view of the neuron differentiation process and allow us to understand the alteration of molecular profiles under both healthy and disease states.

Mutations in the *GRN* gene cause the deficiency of the progranulin (PGRN) protein, which has been linked to various neurodegenerative diseases in the recent decade.[15,16] PGRN is a glycosylated protein composed of multiple granulin modules, each containing a repetitive number of cysteine residues that form disulfide bonds and provide structural stability.[17] After the production of PGRN in ribosomes at the rough endoplasmic reticulum, PGRN is sorted and modified by the Golgi apparatus for its trafficking into the lysosomes and secretion outside of cells.[15] Recent studies have implicated PGRN's role in lysosomal function, protein homeostasis, lipid

Special Issue: Women in Proteomics and Metabolomics

Received: November 15, 2023
Revised: February 7, 2024
Accepted: February 12, 2024

regulation, and neurite outgrowth.[18−21] Our recent study also found that PGRN deficiency neutralizes lysosome pH and influences global protein homeostasis in human neurons.[22] PGRN is involved in multiple organelles and various types of biomolecules, but an integrated proteomics, lipidomics, and metabolomics evaluation has not been reported.

Here we conducted an integrated multiomics study that can identify and quantify proteins, lipids, and metabolites from the same sample with optimal confidence, accuracy, and reproducibility. To understand the molecular profiles of iPSCs and neurons in both healthy and disease states, we used the advanced i^{3}Neuron technology (integrated, inducible, isogenic) which stably integrates the doxycycline (Dox)-inducible Neurogenin 2 (NGN2) transcription factor into the iPSC line and differentiates all iPSCs into a pure population of cortical glutamatergic neurons in 2 weeks.[23,24] This i^{3}Neuron platform provides significantly improved neuron viability, purity, and speed compared to traditional neuron differentiation methods, enabling a scalable and reproducible production of human neurons for omics studies.[22−24] We first compared the proteomics, lipidomics, and metabolomics profiles of healthy wild-type (WT) human iPSCs and i^{3}Neurons. We then investigated how genetic mutations that cause neurodegeneration alter the multiomics molecular profiles of iPSCs and neurons in the context of the *GRN* gene and PGRN deficiency. Loss of *GRN* resulted in distinct changes in iPSCs and neurons, providing key molecular targets and pathways to understand progranulin deficiency in inherited neurodegenerative diseases.

MATERIALS AND METHODS

Human iPSC and iPSC-Derived Neuron Culture

Human iPSCs and iPSC-derived glutamatergic neurons were routinely cultured in our lab using the i^{3}Neuron technology as described previously.[24] Briefly, WT and *GRN*$^{-/-}$ iPSCs with the stably expressed Dox-inducible NGN2 transcription factor were maintained in Essential 8 medium (Gibco) in 10 cm dishes coated with Matrigel (Corning).[22] Neuron differentiation was initiated by replating iPSCs in neuronal induction medium (DMEM/F12 medium, N2 supplement, nonessential amino acid (NEAA), Glutamax, doxycycline) for 3 days. Day 3 neurons were dissociated by Accutase (Gibco) and seeded on 6-well dishes (2 million neurons per well) coated by poly ornithine (Sigma). Neurons were maintained in cortical neuron culture medium (BrainPhys medium, B27 plus supplement, GDNF, BDNF, NT-3, Laminin, and doxycycline) with a half-medium change every other day until day 14. Microscopy images of iPSCs and neurons were taken by using the CELENA S Digital Imaging System (Logos).

Sample Preparation for Multiomics Analysis

Human iPSCs and iPSC-derived neurons (day 14) were harvested at 2 million cell counts in each biological replicate. Before harvesting, the cells were gently washed with phosphate-buffered saline (PBS) twice. Cells were then quenched and harvested by adding 350 μL of an ice-cold methanol/water mixture (5/2, v/v, HPLC grade) directly onto each cell culture plate and scraping into 2 mL tubes. This harvesting step was repeated once and combined into the same tube to minimize cell loss and ensure reproducibility.

Extraction of cellular proteins, lipids, and metabolites was achieved by a methanol/water/chloroform mixture using the Folch method.[25] Internal standards (IS) were added to each tube: $^{13}C_5{}^{15}N$ folic acid (Sigma) for metabolomics and deuterated lipid standards (100 μg/mL, 13 lipid classes) from EquiSplash (Avanti Polar Lipids) for lipidomics (Table S1). Sample tubes were sonicated on ice for 2 min using a Qsonica bath sonicator. Then 1 mL of HPLC grade chloroform was added to each sample, followed by incubation on ice for 1 h with frequent vortexing. Sample tubes were then centrifuged at 12,700 rpm and 4 °C for 15 min. The bottom chloroform layer containing lipids and the top aqueous layer containing metabolites were transferred to separate tubes. The pellet containing the proteins was retained in the original tube. All protein, lipid, and metabolite fractions were dried under SpeedVac.

Dried protein pellets were reconstituted in lysis buffer (8 M urea, 50 mM ammonium bicarbonate (AmBC), and 150 mM sodium chloride), sonicated on ice for 30 min, and clarified by centrifugation, followed by total protein concentration measurements. Proteins were reduced and alkylated by treating with 5 mM tris(2-carboxyethyl)phosphine (TCEP) for 40 min at 37 °C in a Thermomixer (600 rpm), 15 mM iodoacetamide (IAA) for 30 min at 37 °C in dark, and 5 mM dithiothreitol (DTT) for 10 min at 37 °C. AmBC (50 mM) was added to dilute the urea concentration below 1 M. Trypsin/Lys-C mix (Promega) was used for digestion (1:30, w:w) for 16 h at 37 °C. Digestion was quenched by trifluoroacetic acid until pH < 2. Peptide samples were desalted using a Waters HLB 96-well plate following the manufacturer's protocol. Eluted peptide samples were dried, reconstituted in 50 μL of MS grade H_2O, and clarified by centrifugation for nanoLC-MS analysis.

Dried lipid samples were reconstituted in 150 μL of a mixture of methanol/chloroform/water (18/1/1, v/v/v) and clarified by centrifugation for UHPLC-MS/MS analysis. Dried metabolite samples were resuspended in 35 μL of MS grade H_2O with 0.1% formic acid (FA) and clarified by centrifugation for UHPLC-MS/MS analysis. Pooled lipidomics and metabolomics samples were created by combining a small aliquot from each cell type, group, and biological replicate.

LC-MS/MS for Proteomics, Lipidomics, and Metabolomics

Proteomics samples were analyzed on a Dionex Ultimate 3000 RSLCnano system coupled to a Thermo Scientific Q-Exactive HF-X Orbitrap Mass Spectrometer (MS). Mobile phase A was 0.1% FA in MS grade water. Mobile phase B was 0.1% FA in acetonitrile. An Easy-Spray PepMap RSLC C18 column (2 μm, 100 Å, 75 μm × 50 cm) was used for separation in a 210 min gradient at 55 °C and a flow rate of 0.25 μL/min. Data independent acquisition was conducted with an MS scan range of m/z 400 to 1000 in positive ion mode, an MS1 resolving power of 60K, an automatic gain control (AGC) target of 1E6, and a maximum injection time (maxIT) of 60 ms. The precursor isolation window was set at m/z 8.0 (staggered) with 75 sequential DIA MS/MS scans at a MS/MS resolving power of 15K, an AGC target of 2E5, a maxIT of 50 ms, and a normalized collision energy (NCE) of 30%.

Lipid samples were analyzed using a Vanquish Duo UHPLC system coupled with a Thermo Scientific Q-Exactive HF-X MS. Lipids were separated on an ACQUITY UPLC BEH Shield RP18 column (1.7 μm, 2.1 × 150 mm) with a 30 min gradient, 0.15 mL/min flow rate, and 40 °C column temperature. Mobile phase A was water/acetonitrile (9/1, v/v). Mobile phase B was isopropanol/methanol/acetonitrile/water (7/1.5/1/0.5). To facilitate ionization, both mobile phases were supplemented with 0.5 mM NH_4HCO_2 and 5 mM

https://doi.org/10.1021/acs.jproteome.3c00790
J. Proteome Res. XXXX, XXX, XXX−XXX

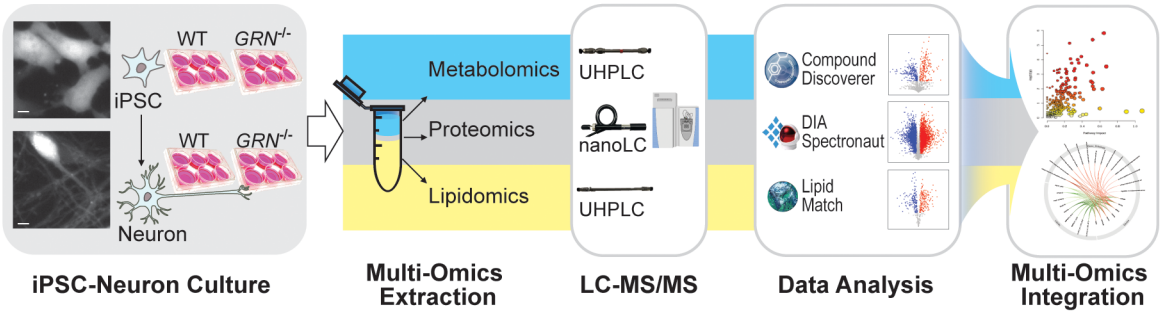

Figure 1. Overall workflow of multiomics analysis in human iPSCs and iPSC-derived neurons. Human iPSCs and iPSC-derived neurons with and without knocking out the *GRN* gene were comparatively evaluated for their protein, lipid, and metabolite profiles. Proteins, lipids, and metabolites were extracted from the same sample using methanol/water/chloroform extraction and analyzed separately on nanoLC-MS/MS and UHPLC-MS/MS platforms. Scale bars in the microscopy images are 5 μm.

NH_4OH. Each sample was analyzed by positive and negative ion modes separately in full MS scans. Pooled iPSC and neuron samples were used for data dependent acquisition (DDA) in both positive and negative ion modes with two technical replicates to obtain MS/MS spectra for confident lipid identification. MS1 scanned from m/z 380 to 1200 (ESI+) or m/z 380 to 2000 (ESI−) with a resolving power 60K and an AGC target of 1E6. DDA used an NCE of 22.5% (ESI+) or 27.5% (ESI−) with a dynamic exclusion time of both 10 and 20 s.

Metabolomics samples were analyzed on the same UHPLC-MS system as for the lipid samples. Metabolites were separated by a Luna Omega Polar C18 column (1.6 μm, 100 Å, 2.1 × 100 mm) with a 10 min gradient, 0.3 mL/min flow rate, 30 °C column temperature, and the same mobile phases as proteomics analysis. Each sample was analyzed in full MS mode for both positive and negative ESI, and pooled samples were analyzed in DDA mode for identification purposes. MS1 scanned from m/z 70 to 800 with a resolving power of 60K and an AGC target of 1E6. DDA used an NCE of 30% and a dynamic exclusion time of 10 s.

Multiomics Data Analysis

The DIA proteomics data was analyzed by the Spectronaut software (v18.1, Biognosys) under default settings with DirectDIA mode. The Swiss-Prot *Homo sapiens* reviewed database and our newly built contaminant libraries (https://github.com/HaoGroup-ProtContLib)[26] were included for protein identification. Up to two missed cleavages and three variable modifications were allowed. Carbamidomethyl C was set as the fixed modification, and methionine oxidation and protein N-terminal acetylation were set as variable modifications. False discovery rates (FDR) for precursors and proteins were set at 0.01. DIA precursor intensities below 1000 were removed for better confidence. To reduce variations, proteomics data from the same total protein amount were further normalized by total spectral abundance from each sample within the same cell type.

Lipidomics data was analyzed by the LipidMatch software (v4.0).[27] Lipids were identified with a 5 ppm mass tolerance for precursor ions and 10 ppm for product ions. Lipid peak areas were normalized both by the lipid internal standard from each lipid class and by the total protein amount from each sample. Semi-absolute quantification was achieved with the lipid internal standards from each lipid class (pmol lipid per μg of protein) using a method described elsewhere.[28] For lipid annotation, an underbar "_" was used between the acyl chain composition for glycerophospholipids (GPs) and glycerolipids (GLs) without exact acyl chain locations. For the sphingolipid (SP), "/" was used between the sphingosine backbone and acyl chain composition with the exact acyl chain location.

Metabolomics data was analyzed by the Compound Discoverer software (v3.3, Thermo). Metabolite identification was achieved by MS1 and MS/MS database searches with the built-in MzCloud, ChemSpider, HMDB, KEGG libraries, and our in-house metabolite standard spectral library.[29,30] Parameters included a maximum retention time shift of 0.5 min, a mass tolerance of 10 ppm, and a minimum peak intensity of 1E5. Key metabolite quantifications were further confirmed by Skyline software[31] for targeted peak extraction and integration. Metabolite peak areas were normalized both by the internal standard to reduce instrumental variation and by the total protein amount from each sample to reduce cell material variation.

Statistical analysis for proteomics data was conducted with Spectronaut software. Statistical analyses for lipidomics and metabolomics were conducted by t tests in R. Several other software packages were used for further data analysis: VolcaNoseR[32] for volcano plots, ShinyGO[33] for protein GO-enrichment analysis, LION[34] for lipid GO-enrichment analysis, MBRole3[35] for metabolite GO-enrichment analysis, LINT[11] for proteomics and lipidomics network analysis, Metaboanalyst[10] for principal component analysis (PCA), and joint proteomics and metabolomics pathway analysis.

RESULTS AND DISCUSSION

Establishing a Multiomics Workflow for Human iPSCs and iPSC-Derived Neurons

We established an integrated proteomics, lipidomics, and metabolomics workflow for human iPSCs and iPSC-derived neurons, as illustrated in Figure 1. Example LC-MS chromatograms for proteomics, lipidomics, and metabolomics are provided in Figure S1. Confident protein analysis was achieved by abundance and FDR filtering as well as our newly established contaminant libraries.[26] Confident lipid and metabolite identification were achieved by MS1 and MS/MS matching to online databases as well as retention time matching to our in-house spectral library that contains 13 lipid classes and 90 metabolite standards. Semi-absolute quantification for lipidomics (pmol lipid per μg of protein) was achieved with IS from 13 lipid classes using a method described elsewhere.[28] We first validated this method using the pooled lipid samples with spiked-in IS before extraction,

https://doi.org/10.1021/acs.jproteome.3c00790
J. Proteome Res. XXXX, XXX, XXX−XXX

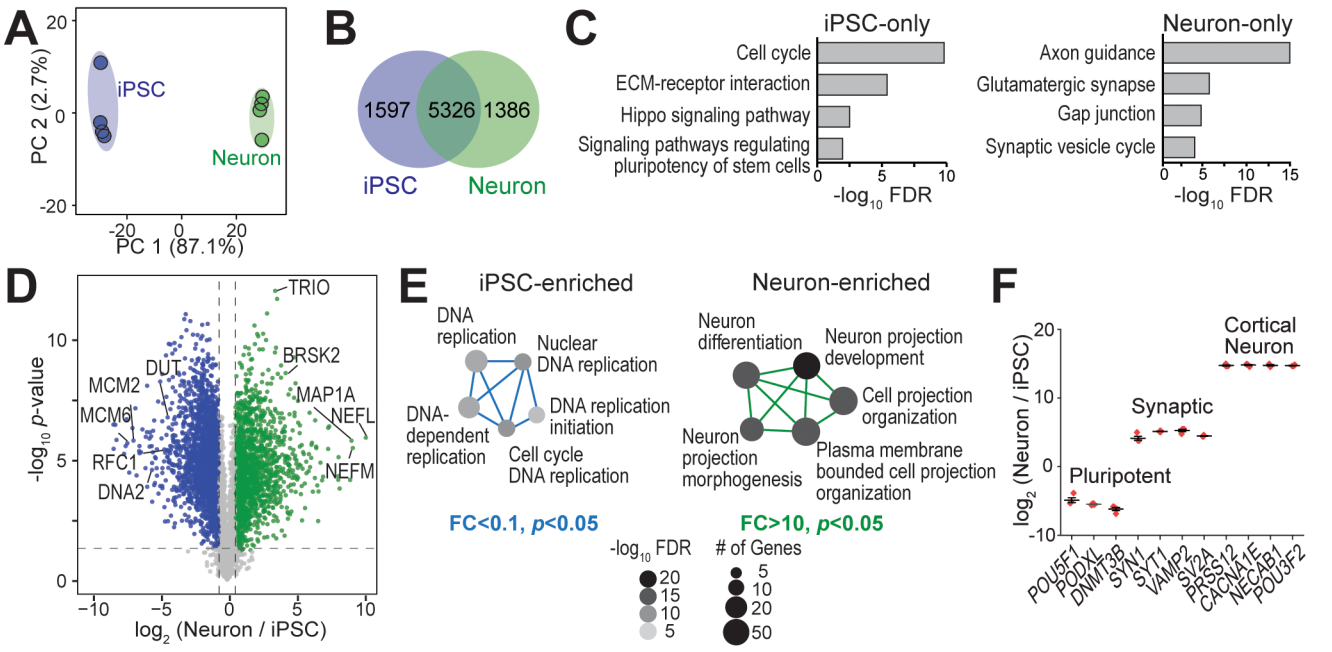

Figure 2. Proteomics evaluation of healthy human iPSCs vs i^{3}Neurons. (A) Principal component analysis of proteomics data sets from iPSC and neuron groups, each with four biological replicates. (B) Venn diagram of reproducibly quantified proteins in iPSC and neuron groups with at least three replicates in one group. (C) KEGG pathways enriched from proteins quantified in iPSC-only and neuron-only groups. (D) Proteomics volcano plot. Dashed lines denote a *p*-value of 0.05 and a fold change of 1.5. (E) Biological processes enriched from significantly altered proteins in iPSCs and neurons. FC denotes neuron/iPSC ratio. (F) Significant changes of protein markers for pluripotent, synaptic, and cortical neurons.

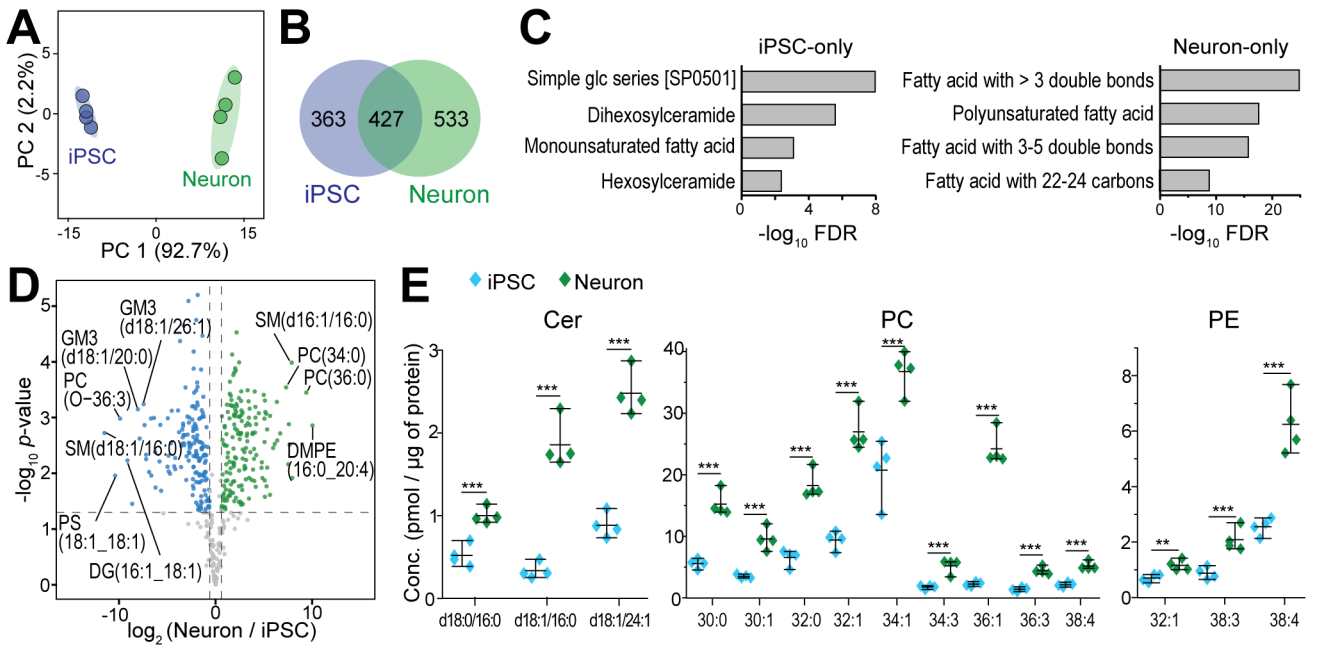

Figure 3. Lipidomics evaluation of healthy human iPSCs vs neurons. (A) Principal component analysis of lipidomics data sets from iPSCs and neurons. (B) Venn diagram of reproducibly quantified lipids in iPSC and neuron groups. (C) KEGG pathways enriched from lipids quantified in iPSC-only and neuron-only groups. (D) Lipidomics volcano plot. (E) Key lipid concentrations measured by semi-absolute quantification method in iPSCs vs neurons (* denotes $p < 0.05$, ** denotes $p < 0.01$, and *** denotes $p < 0.001$).

achieving excellent recovery (average = 94.0%), a minimal matrix effect (average = −2.4%), and reproducible retention times (RSD = 0.1%) (Tables S1 and S2). With this integrated multiomics workflow, we confidently identified and quantified a total of 8309 proteins, 1323 lipids, and 472 metabolites from human iPSCs and neurons (16 data sets × 3 omics types).

Proteomics, Lipidomics, and Metabolomics Profiles of Healthy iPSCs and i^{3}Neurons

To understand the stem cell and neuron biology as well as the differentiation process, we compared the proteomics, lipidomics, and metabolomics profiles of healthy WT human iPSCs and iPSC-derived i^{3}Neurons. Principal component analysis

https://doi.org/10.1021/acs.jproteome.3c00790
J. Proteome Res. XXXX, XXX, XXX−XXX

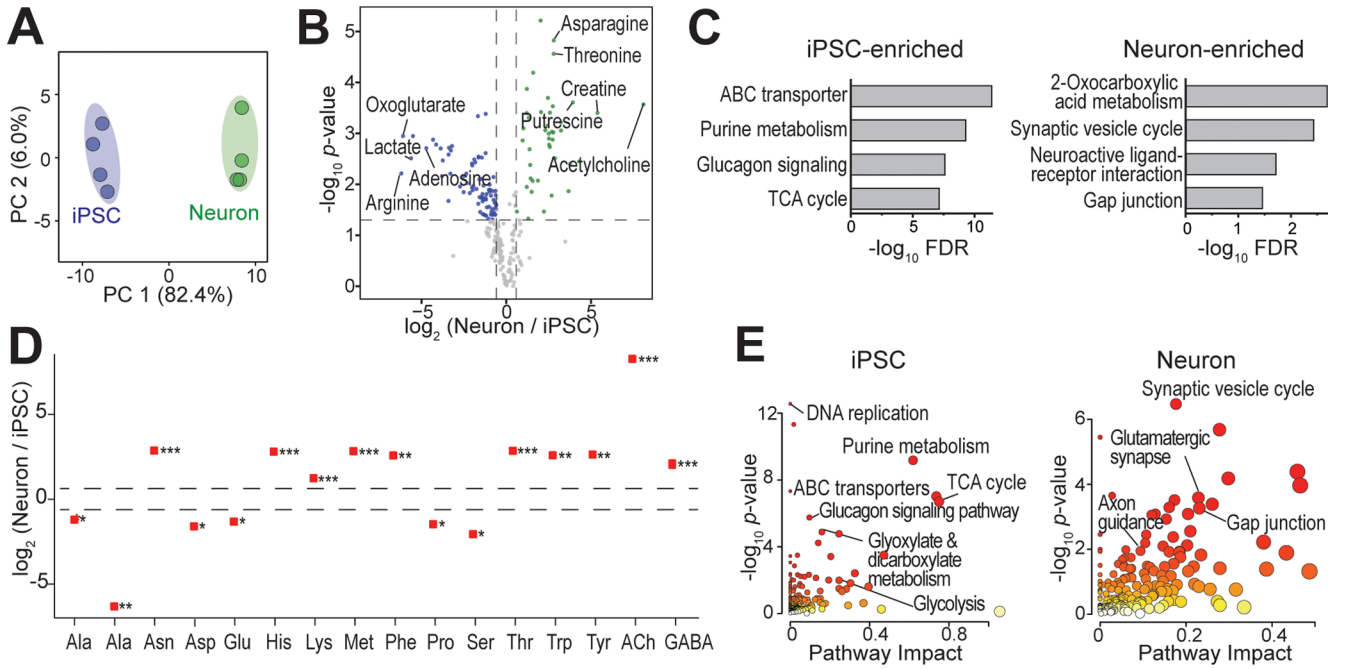

Figure 4. Metabolomics and multiomics evaluation of healthy human iPSCs vs neurons. (A) Principal component analysis of metabolomics data sets from iPSCs and neurons. (B) Metabolomics volcano plot. (C) KEGG pathways enriched from differentially regulated metabolites in iPSCs vs neurons. (D) Abundance changes of amino acids and neurotransmitters. (E) Joint KEGG pathway analysis using significantly altered proteins and metabolites.

(PCA) achieved complete separation between iPSC and neuron cell types in each omics data set (Figure 2A, Figure 3A, and Figure 4A). In proteomics data, a total of 8309 proteins were identified and quantified, in which 5326 proteins were reproducibly quantified in both WT iPSC and neuron groups (Figure 2B). Proteins uniquely quantified in the iPSC cell type were related to cell cycle, ECM−receptor interactions, and signaling pathways regulating stem cell proliferation (Hippo signaling) and pluripotency (Figure 2C).[36] Proteins uniquely quantified in neurons were related to synapse, axon, and interneuron communication (gap junction).[37] This reflected the unique nature of stem cells that undergo mitosis, while mature neurons do not divide and develop long axons and synapses for neuronal firing. It is worth noting that unquantified molecules from one cell type could be low-abundance and below the detection limit rather than completely absent from the cell. The quantitative comparison of shared molecules in iPSC and neuron cell types was further illustrated in Figure 2D. GO-enrichment analysis showed significantly enriched DNA replication processes in iPSCs (e.g., MCM6, MCM2, DNA2, RCF1, and DUT) and neuron projection processes in neurons (e.g., BRSK2, TRIO, and MAP1A) (Figure 2E). Neurofilament proteins (NEFL, NEFM, and NEFH) that support axon structures are among the highest up-regulated proteins in neurons. Key protein markers for pluripotency were enriched in iPSCs, while synaptic and cortical neuron markers were enriched in neurons (Figure 2F), validating the successful neuron differentiation in our iPSC−neuron platform.

In lipidomics data, a total of 1323 lipids were identified and quantified, in which 427 lipids were quantified in both WT iPSC and neuron groups (343 glycerophospholipids (GP), 48 sphingolipids (SP), 30 glycerolipids (GL), and 6 sterol lipids (ST)) (Figure 3B). Lipids uniquely identified in iPSCs were simple glc series, monounsaturated fatty acids, and glycosphingolipids (hexosylceramide) (Figure 3C). Monounsaturated fatty acids are key precursors to maintain stem cell growth and cell structure.[38] A high concentration of glycosphingolipids is a unique characteristic for stem cells and is important for cell adhesion.[39] For neuron-specific lipids, polyunsaturated fatty acids (PUFA) were enriched, which are known to be related to synapses and neuron communication.[40] Neuron differentiation significantly altered lipid composition and abundances (Figure 3D and Figure S2A). Phosphatidylcholine (PC) was still the most abundant lipid class in both cell types. The total amount of ganglioside (GM) was decreased more than 90% in neurons (Figure S2B). This dramatic change of gangliosides could be regulated by stage-specific gene expressions during neuron differentiation.[41] Additionally, neurons have 1.5-fold higher ($p < 0.01$) amount of total cardiolipin (CL) and 1.6-fold more CL species containing 16:0 or 18:1 fatty acyl chain compared to iPSCs, which is likely due to CL's role in axon generation (Supplementary Data and Figure S2B).[42] Increased CL and ceramide (Cer) have been previously indicated to promote neuron differentiation (Figure 3E).[43,44] We also found significantly increased PC and phosphatidylethanolamine (PE) in neurons compared to iPSCs, which may be explained by the increased cell surface in polarized neurons, as PC and PE are main components of the cell membrane.[45]

Untargeted metabolomics identified and quantified a total of 472 metabolites from iPSCs and neurons (Figures 4A and 4B). Because most small molecular metabolites are shared across different cell types and organisms, we used differentially regulated metabolites for enrichment analysis (Figure 4C). ABC transporters were enriched in iPSCs, which are essential for stem cell proliferation and self-renewal.[46] Purine metabolism, the glucagon signaling pathway, and the TCA cycle were also enriched in iPSCs, which are related to stem cell energy production through glycolysis and the TCA cycle.[47] As

https://doi.org/10.1021/acs.jproteome.3c00790
J. Proteome Res. XXXX, XXX, XXX−XXX

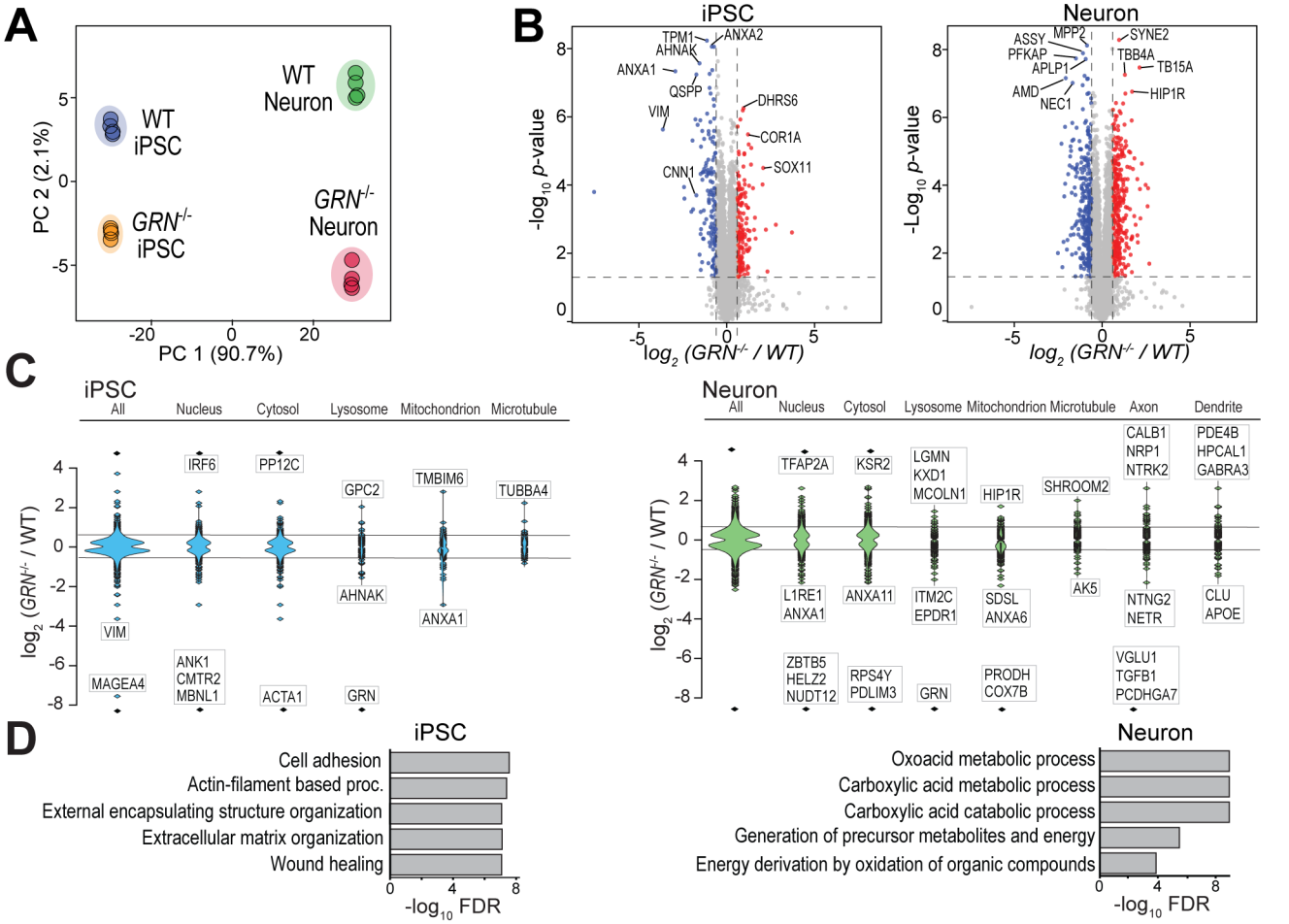

Figure 5. Proteomic alterations of $GRN^{-/-}$ iPSCs and neurons compared to WT. (A) Principal component analysis from proteomic data sets. (B) Volcano plots of $GRN^{-/-}$ vs WT groups in iPSCs and neurons. (C) Violin plots of protein changes from different subcellular locations. Proteins that were only quantified in one group were shown as outliers. (D) GO-enrichment analysis of significantly decreased proteins in $GRN^{-/-}$ vs WT iPSCs and neurons.

expected, metabolites related to the synaptic vesicle cycle, neuroactive ligand−receptor interactions, and gap junctions were enriched in neurons.[48] The differences of amino acids and neurotransmitters in iPSCs vs neurons are illustrated in Figure 4D. Most neurotransmitters were increased in neurons as expected. Acetylcholine was increased by over 100-fold in neurons, which is known to regulate neuronal networks.[49] Alanine was significantly lower in neurons vs iPSCs, likely due to its central role in TCA cycles in stem cells.[50] We also conducted joint pathway analysis using significantly changed proteins and metabolites, revealing stem-cell- and neuron-specific metabolic pathways (Figure 4E). Taken together, our multiomics platform has identified and quantified unique molecular profiles related to stem cell and neuron biology, which can help us understand the neuron differentiation process.

Proteomics, Lipidomics, and Metabolomics Evaluation of Progranulin Deficiency in iPSCs and Neurons

After obtaining the multiomics profiles of WT iPSCs and neurons, we hope to further examine how genetic mutations alter molecular profiles in stem cells and neurons. Using our *GRN* knockout iPSC and neuron model of neurodegeneration, we first examined whole cell proteomics in $GRN^{-/-}$ vs WT iPSCs and neurons. A PCA plot shows clustered proteomics data based on cell type and genotype (Figure 5A). The PGRN protein was absent from the $GRN^{-/-}$ group in both iPSCs and neurons, confirming the knocking out efficiency. Loss of *GRN* seem to influence neuronal proteins more than iPSCs with 5.2% significantly changed proteins in neurons and 2.7% in iPSCs (>1.5 fold-change and $p < 0.05$) (Figure 5B). In iPSCs, PGRN loss affected focal adhesion, actins (ANXA1 and AHNAK), and cytoskeleton proteins (CNN1, AHNAK, and VIM) (Figure 5B). In neurons, we observed a significant loss of postsynaptic proteins (MPP2 and APLP1), consistent with the potential role of PGRN in neurite outgrowth.[20,51] PGRN is trafficked into lysosomes and secreted outside of cells, involving multiple organelles in this process.[15] Grouping proteins based on their known subcellular locations showed that many proteins were altered in $GRN^{-/-}$ neurons from the lysosome, mitochondrion, axon, and dendrite (Figure 5C). GO-enrichment analysis of significantly down-regulated proteins in iPSCs and neurons confirmed PGRN's roles in cellular inflammation and wound repair, also implicating the undiscovered roles of PGRN in metabolic and catabolic process of small molecules, such as carboxylic acids and carbohydrates (Figure 5D).[15]

PGRN deficiency has recently been linked to lipid dysregulation.[21,52] The PCA plot showed complete separation of lipid profiles based on cell type and genotype, similar to

https://doi.org/10.1021/acs.jproteome.3c00790
J. Proteome Res. XXXX, XXX, XXX−XXX

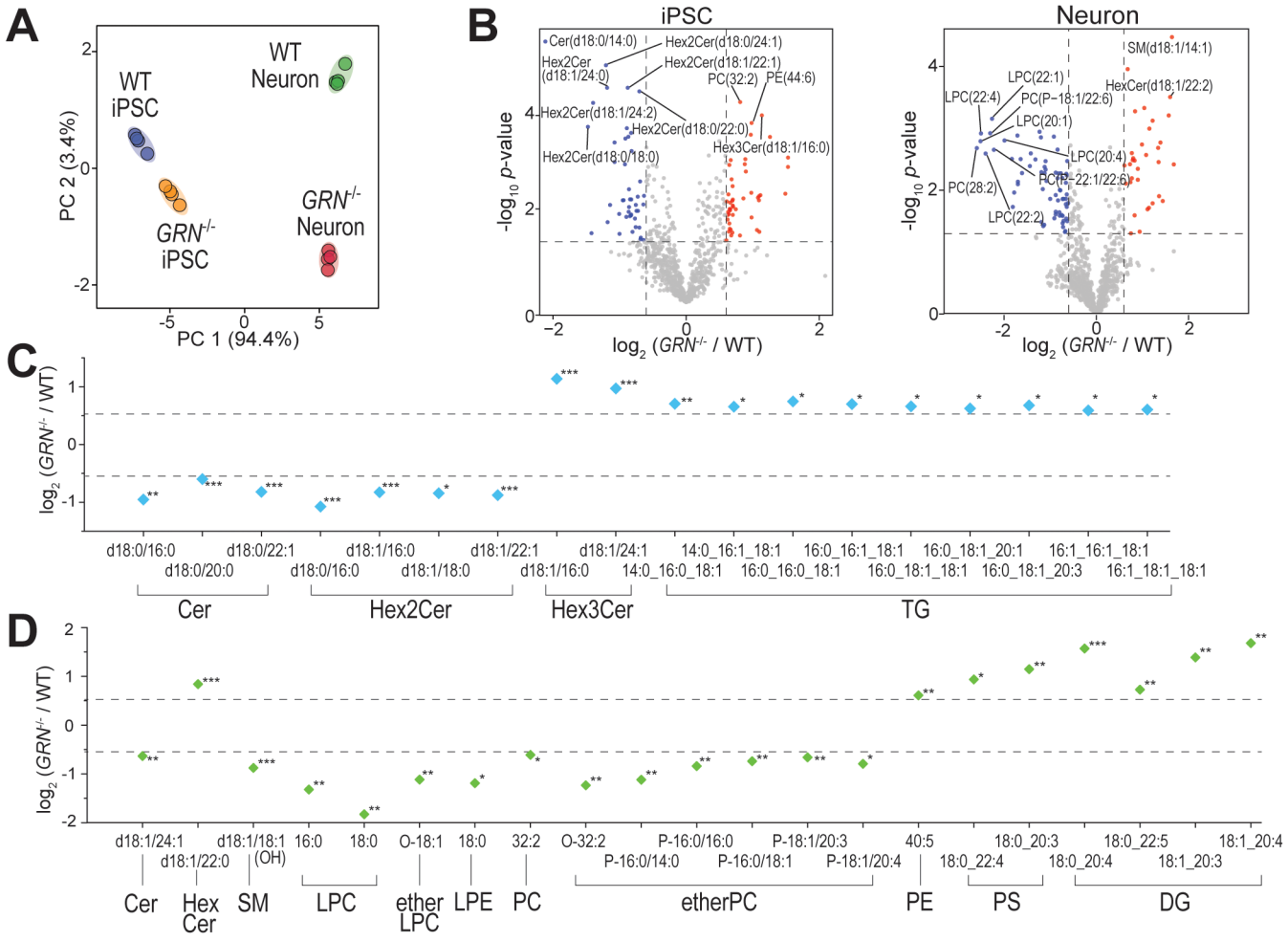

Figure 6. Lipidomic alterations of $GRN^{-/-}$ iPSCs and neurons compared to WT. (A) Principal component analysis from lipidomic data sets. (B) Volcano plots of $GRN^{-/-}$ vs WT groups in iPSCs and neurons. (C) Key lipid changes in iPSCs. (D) Key lipid changes in neurons.

proteomics results (Figure 6A). In iPSCs, significantly changed lipid species were shown in Figures 6B and 6C. Among them, triacylglycerols (TG) was the most influenced lipid class, which is important for energy storage and mitochondrial function.[53] Interestingly, most dihexosylceramide (Hex2Cer) species were down-regulated, and trihexosylceramide (Hex3Cer) species were up-regulated in $GRN^{-/-}$ vs WT iPSCs. Hex2Cer is related to cell proliferation and Hex3Cer is related to neuronal inflammation.[54] Cer can regulate inflammation and binds to cathepsin, which cleaves PGRN into individual granulin peptides inside the lysosome.[55,56] In $GRN^{-/-}$ neurons, over 100 lipid species were significantly changed, such as SP, GP, and GL (Figure 6D and Figure S3A). Ether lipids (ether lysoPC (LPC) and ether PC) were significantly decreased in $GRN^{-/-}$ vs WT, which may relate to their roles as antioxidants in the central nervous system.[57] Particularly, LPC/PC ratios were decreased in both iPSCs (ratio = 0.9) and neurons (ratio = 0.3) (Figure S3B). This finding is especially significant because reduced LPC/PC ratios have been used to implicate impaired brain function but have not been reported in progranulin deficiency.[58] Taken together, we found that PGRN deficiency influenced different lipid species in iPSCs and neurons and caused more dramatic lipid alterations in neurons compared to those in iPSCs, indicating the important and distinct roles of PGRN in different cell types.

To the best of our knowledge, metabolomics changes have never been characterized in progranulin-deficient cells. Using the 472 identified and quantified metabolites in our untargeted metabolomics data, we achieved complete PCA separation based on cell type and genotype. In iPSCs, less than 20 metabolites were significantly altered (ten increased and three decreased) by the loss of PGRN. On the other hand, over 150 metabolites were significantly altered in $GRN^{-/-}$ vs WT neurons. Key metabolite changes are illustrated in Figures 7C and 7D. Amino acids were not changed in the $GRN^{-/-}$ iPSCs. In contrast, glutamine and serine were significantly increased, and histidine, lysine, methionine, phenylalanine, threonine, tryptophan, and tyrosine were significantly decreased in $GRN^{-/-}$ neurons. Excessive glutamine was previously reported to cause neurotoxicity due to the hyperammonemia condition.[59] The accumulated succinate, fumarate, and malate in $GRN^{-/-}$ neurons could lead to DNA hypermethylation, which is related to neurodegeneration.[60,61] Creatinine, a potential biomarker for various neurodegenerative diseases, was significantly increased in $GRN^{-/-}$ neurons.[62] We also evaluated purine and pyrimidine metabolites since down-regulated purine and pyrimidine metabolism pathways have been reported to correlate with neurodegeneration.[63] In iPSCs, only cytidine in this pathway was significantly decreased (Figure 7C), while in neurons, six purine metabolites (*S*-adenosylhomocysteine, xanthine, xanthosine, CDP-choline,

https://doi.org/10.1021/acs.jproteome.3c00790
J. Proteome Res. XXXX, XXX, XXX−XXX

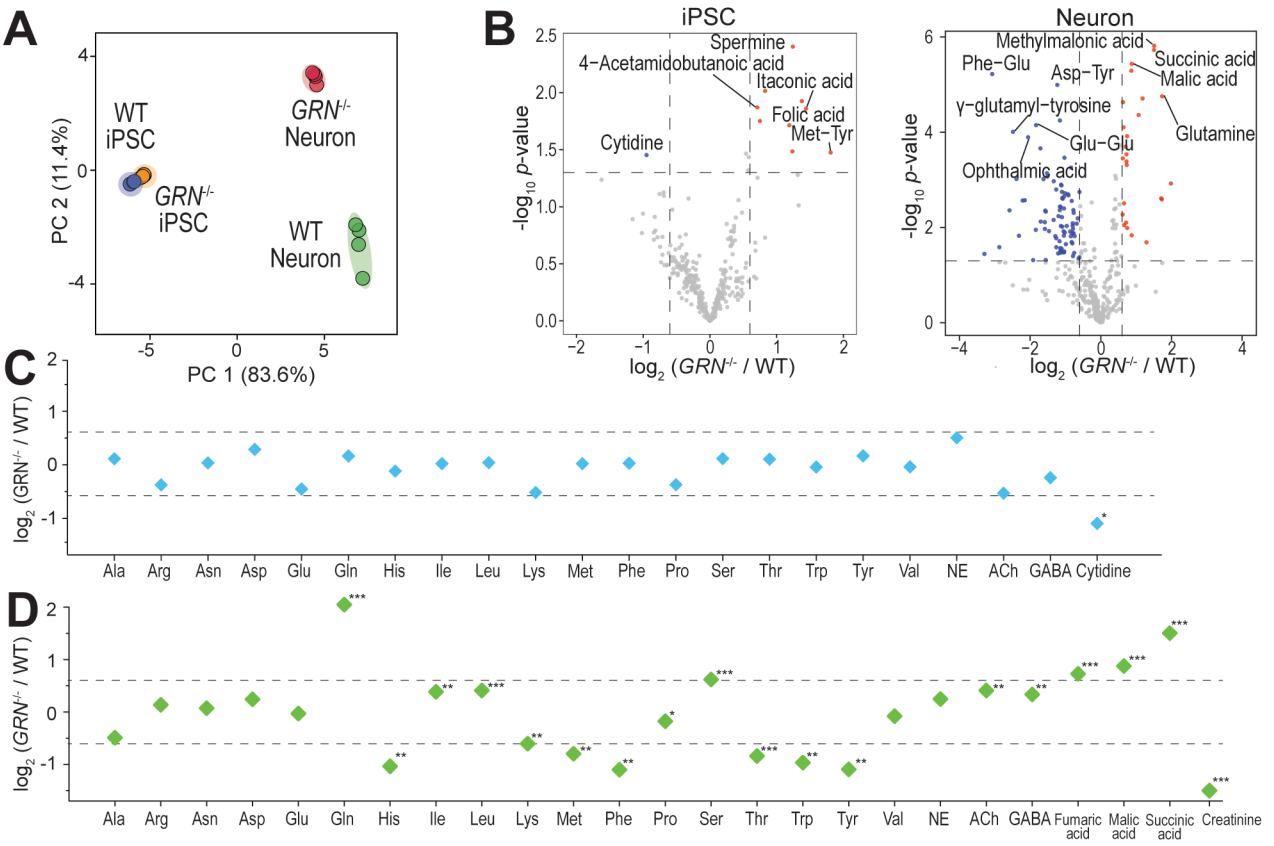

Figure 7. Metabolomics alterations of $GRN^{-/-}$ iPSCs and neurons compared to WT. (A) Principal component analysis from metabolomics data sets. (B) Volcano plots of $GRN^{-/-}$ vs WT groups in iPSCs and neurons. (C) Key metabolite changes in iPSCs. (D) Key metabolite changes in neurons.

deoxycytidine, and zalcitabine) were significantly decreased (Figure S4). Cytidine is essential for the synthesis of PC and PE in the brain through the Kennedy cycle, representing a pivotal pathway for the generation of PUFA.[64] Taken together, we found that the loss of PGRN influenced neuronal metabolite profiles more severely than iPSCs, and many metabolites that are crucial to neuron functions were significantly altered in neurons.

Integrated Multiomics Evaluation of Progranulin-Deficient Neurons

To obtain a holistic view of PGRN deficiency in neurons, we conducted multiomics integration to integrate proteins, lipids, and metabolites into the same biological pathways and processes. Since our multiomics data suggested that neurons are more vulnerable to PGRN deficiency compared to iPSCs, we focused on the neuron cell type here. Integrating protein and lipid changes by LINT-WEB[11] with K-mean clustering enriched biological processes related to neuron projection and axon guidance (Figure 8A). Diacylglycerol (DG) is the most abundant lipid class in this cluster and was reported to be essential for the neurite spine formation.[65] Bis-(monoacylglycerol)phosphate (BMP) is essential to support lysosomal membrane functions and has been reported to be linked to PGRN deficiency.[21] Integrating metabolite and protein changes in Metaboanalyst[10] resulted in enriched KEGG pathways, such as axon guidance, glutamatergic synapses, lysosomes, the TCA cycle, and tight junctions (Figure 8B). Many of these pathways have been reported to regulate neuroprotection.[66] Glutamate can induce neurotoxicity, and lactate and cysteine are neuroprotective factors.[67] Notably, GRM8, NRP1, PDE4B, and PRKCE proteins were selected in both LINT-WEB and Metaboanalyst. The selected DG 38:4 (18:0_20:4 and 18:1_20:3) and PE 42:9 lipids were highly correlated with these four proteins ($\rho > 0.8$). GRM8 is a neuronal metabotropic glutamate receptor that responds to neuroinflammation and is significantly increased in $GRN^{-/-}$ neurons.[68] Phosphodiesterases (PDE4s) are expressed in neurons and hydrolyze cAMP in purine metabolism, a promising drug target for brain diseases.[69] Interestingly, both PDE4B and PDE4D were up-regulated, but a majority of purine metabolites were down-regulated in our data. Overall, many pathways commonly emerged as synaptic dysfunctions and axon guidance in our multiomics integration, indicating PGRN's role in synaptic function and brain metabolism.

CONCLUSIONS

In summary, we conducted a multiomics analysis of human iPSCs and iPSC-derived neurons, integrating proteomics, lipidomics, and metabolomics with optimal identification confidence, quantification accuracy, and reproducibility. Using this integrated multiomics method, we discovered unique molecular profiles in iPSCs and neurons that are important to stem cell and neuron biology as well as neuron differentiation. We also found that the loss of the *GRN* gene resulted in distinct changes in iPSC and neuron cell types. Proteins and lipids in iPSCs showed changes related to wound healing, extracellular matrix organization, and mitochondrial function, whereas neurons had more dramatic metabolite and

https://doi.org/10.1021/acs.jproteome.3c00790
J. Proteome Res. XXXX, XXX, XXX−XXX

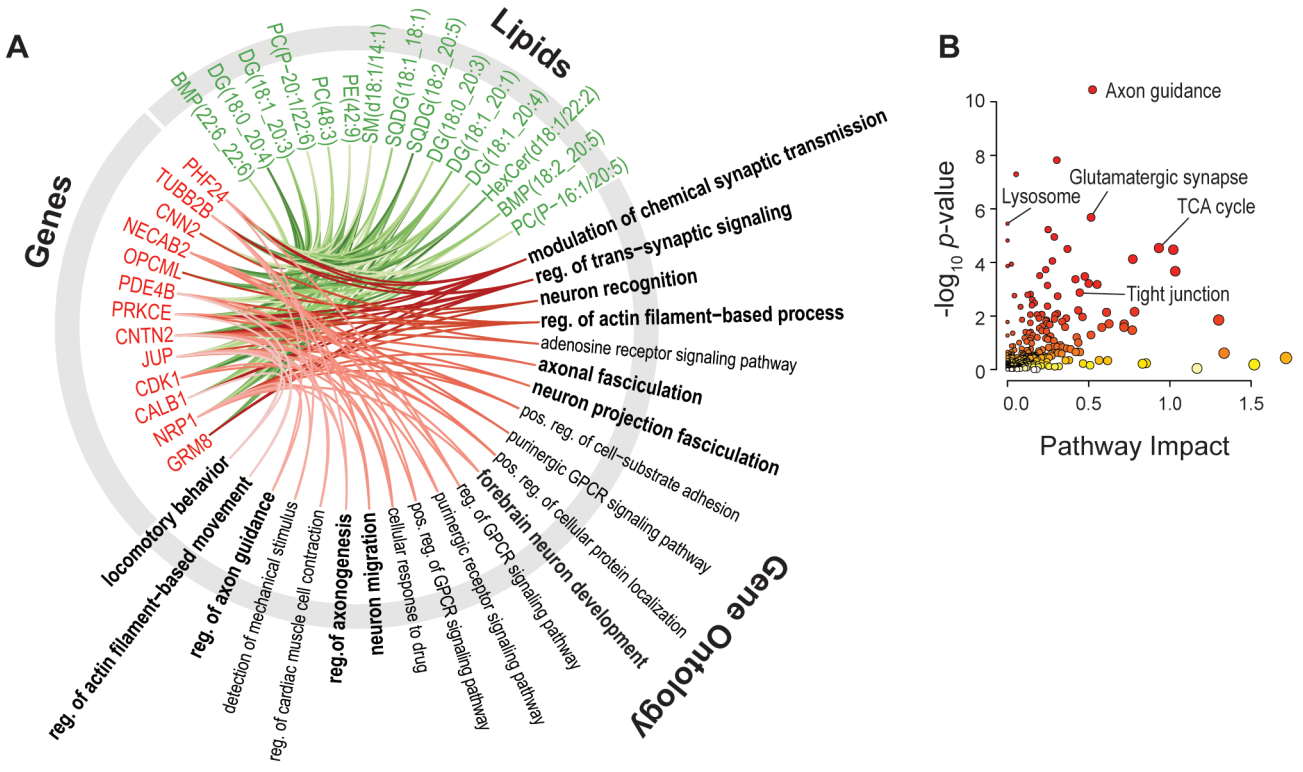

Figure 8. Integrated multiomics analyses of $GRN^{-/-}$ vs WT neurons. (A) Significantly altered biological processes and related protein (red) and lipid (green) changes in $GRN^{-/-}$ vs WT neurons from LINT-WEB network analysis. The red lines represent the correlation between Gene ID and GO terms, and the green lines represent the correlation between gene ID and lipids. (B) Joint KEGG pathway analysis using proteomics and metabolomics data from $GRN^{-/-}$ vs WT neurons.

neurotransmitter changes as well as protein and lipid changes related to neuron projection and brain metabolism. Our multiomics results pointed toward the same hypothesis that neurons seem to be more vulnerable to PGRN deficiency compared to stem cells, consistent with the neurological symptoms and cognitive impairment from patients carrying inherited *GRN* mutations. However, this study also has limitations. Our experiments were conducted on the whole-cell scale, which may not illustrate the specific changes from individual organelles. Lysosome-specific protein and lipid changes discovered in isolated intact lysosomes from other PGRN studies seemed to be buried when we homogenized whole cells. Protein trafficking and molecular interactions across multiple subcellular components cannot be captured in whole-cell omics and need to be studied with organelle-specific probes, immunoprecipitation, or proximity labeling. Despite these limitations, our integrated multiomics analyses provided a holistic view of the differences between iPSCs and neurons as well as the whole-cell level impact of progranulin deficiency on iPSCs and neurons to understand neuron differentiation and inherited neurodegenerative diseases.

■ ASSOCIATED CONTENT

Data Availability Statement

Raw LC-MS/MS data from this manuscript are available through the MassIVE repository (identifier: MSV000093388).

Supporting Information

The Supporting Information is available free of charge at https://pubs.acs.org/doi/10.1021/acs.jproteome.3c00790.

The list of internal standards for lipidomics and metabolomics (Table S1); method validation for lipidomics using internal standards from 13 lipid classes (Table S2); example LC-MS chromatograms from proteomics, lipidomics, and metabolomics (Figure S1); lipid changes between WT iPSCs and neurons (Figure S2); lipid changes between $GRN^{-/-}$ vs WT iPSCs and neurons (Figure S3); and metabolite changes related to purine and pyrimidine metabolic pathways in $GRN^{-/-}$ vs WT neurons (Figure S4) (PDF)

The complete data sets for quantitative proteomics, lipidomics, and metabolomics in WT and $GRN^{-/-}$ iPSCs and neurons (XLSX)

■ AUTHOR INFORMATION

Corresponding Author

Ling Hao − *Department of Chemistry, The George Washington University, Washington, D.C. 20052, United States;* orcid.org/0000-0002-0106-5266; Phone: +1 (202) 994-4492; Email: linghao@gwu.edu

Authors

Gwang Bin Lee − *Department of Chemistry, The George Washington University, Washington, D.C. 20052, United States*

Wan Nur Atiqah binti Mazli − *Department of Chemistry, The George Washington University, Washington, D.C. 20052, United States;* orcid.org/0009-0003-2725-6671

Complete contact information is available at: https://pubs.acs.org/10.1021/acs.jproteome.3c00790

https://doi.org/10.1021/acs.jproteome.3c00790
J. Proteome Res. XXXX, XXX, XXX−XXX

Author Contributions

#G.L. and W.M. are co-first authors. G.L., W.M., and L.H. designed the study. W.M. cultured iPSCs and neurons. G.L. conducted sample preparation and LC-MS analysis. G.L. and W.M. analyzed the data and wrote the manuscript with edits from L.H. All authors have read and approved the final manuscript.

Notes

The authors declare no competing financial interest.

■ ACKNOWLEDGMENTS

This study is supported by the NIH grant (R01NS121608, L.H.). The authors would like to acknowledge Dr. Michael Ward from NINDS for providing the iPSC cell lines, Jiawei Ni from the Hao Lab for taking microscopy images, and Ashley Frankenfield from the Hao Lab for insights on Spectronaut data analysis. We thank all of the Hao Lab members for their support and friendship.

■ REFERENCES

(1) Takahashi, K.; Tanabe, K.; Ohnuki, M.; Narita, M.; Ichisaka, T.; Tomoda, K.; Yamanaka, S. Induction of Pluripotent Stem Cells from Adult Human Fibroblasts by Defined Factors. *Cell* **2007**, *131* (5), 861−872.

(2) Dolmetsch, R.; Geschwind, D. H. The Human Brain in a Dish: The Promise of iPSC-Derived Neurons. *Cell* **2011**, *145* (6), 831−834.

(3) Lu, J.; Zhong, X.; Liu, H.; Hao, L.; Huang, C. T.-L.; Sherafat, M. A.; Jones, J.; Ayala, M.; Li, L.; Zhang, S.-C. Generation of Serotonin Neurons from Human Pluripotent Stem Cells. *Nat. Biotechnol.* **2016**, *34* (1), 89−94.

(4) Varderidou-Minasian, S.; Verheijen, B. M.; Schatzle, P.; Hoogenraad, C. C.; Pasterkamp, R. J.; Altelaar, M. Deciphering the Proteome Dynamics during Development of Neurons Derived from Induced Pluripotent Stem Cells. *J. Proteome Res.* **2020**, *19* (6), 2391−2403.

(5) Panopoulos, A. D.; Yanes, O.; Ruiz, S.; Kida, Y. S.; Diep, D.; Tautenhahn, R.; Herrerías, A.; Batchelder, E. M.; Plongthongkum, N.; Lutz, M.; Berggren, W. T.; Zhang, K.; Evans, R. M.; Siuzdak, G.; Belmonte, J. C. I. The Metabolome of Induced Pluripotent Stem Cells Reveals Metabolic Changes Occurring in Somatic Cell Reprogramming. *Cell Res.* **2012**, *22* (1), 168−177.

(6) Lee, H.; Lee, J. J.; Park, N. Y.; Dubey, S. K.; Kim, T.; Ruan, K.; Lim, S. B.; Park, S.-H.; Ha, S.; Kovlyagina, I.; Kim, K.-t.; Kim, S.; Oh, Y.; Kim, H.; Kang, S.-U.; Song, M.-R.; Lloyd, T. E.; Maragakis, N. J.; Hong, Y. B.; Eoh, H.; Lee, G. Multi-Omic Analysis of Selectively Vulnerable Motor Neuron Subtypes Implicates Altered Lipid Metabolism in ALS. *Nat. Neurosci* **2021**, *24* (12), 1673−1685.

(7) Reilly, L.; Lara, E.; Ramos, D.; Li, Z.; Pantazis, C. B.; Stadler, J.; Santiana, M.; Roberts, J.; Faghri, F.; Hao, Y.; Nalls, M. A.; Narayan, P.; Liu, Y.; Singleton, A. B.; Cookson, M. R.; Ward, M. E.; Qi, Y. A. A Fully Automated FAIMS-DIA Proteomic Pipeline for High-Throughput Characterization of iPSC-Derived Neurons. *Cell Reports Methods* **2023**, *3* (10), No. 100593.

(8) Kapoor, M.; Chao, M. J.; Johnson, E. C.; Novikova, G.; Lai, D.; Meyers, J. L.; Schulman, J.; Nurnberger, J. I.; Porjesz, B.; Liu, Y.; Hesselbrock, V.; Kuperman, S.; Kramer, J.; Kamarajan, C.; Pandey, A.; Bierut, L.; Rice, J. P.; Bucholz, K. K.; Schuckit, M.; Tischfield, J.; Brooks, A.; Hart, R. P.; Almasy, L.; Dick, D.; Salvatore, J.; Slesinger, P.; Foroud, T.; Edenberg, H. J.; Marcora, E.; Agrawal, A.; Goate, A. Multi-Omics Integration Analysis Identifies Novel Genes for Alcoholism with Potential Overlap with Neurodegenerative Diseases. *Nat. Commun.* **2021**, *12* (1), n/a.

(9) Li, J.; Lim, R. G.; Kaye, J. A.; Dardov, V.; Coyne, A. N.; Wu, J.; Milani, P.; Cheng, A.; Thompson, T. G.; Ornelas, L.; Frank, A.; Adam, M.; Banuelos, M. G.; Casale, M.; Cox, V.; Escalante-Chong, R.; Daigle, J. G.; Gomez, E.; Hayes, L.; Holewenski, R.; Lei, S.; Lenail, A.; Lima, L.; Mandefro, B.; Matlock, A.; Panther, L.; Patel-Murray, N. L.; Pham, J.; Ramamoorthy, D.; Sachs, K.; Shelley, B.; Stocksdale, J.; Trost, H.; Wilhelm, M.; Venkatraman, V.; Wassie, B. T.; Wyman, S.; Yang, S.; Van Eyk, J. E.; Lloyd, T. E.; Finkbeiner, S.; Fraenkel, E.; Rothstein, J. D.; Sareen, D.; Svendsen, C. N.; Thompson, L. M.; Phatnani, H.; Kwan, J.; Sareen, D.; Broach, J. R.; Simmons, Z.; Arcila-Londono, X.; Lee, E. B.; Van Deerlin, V. M.; Shneider, N. A.; Fraenkel, E.; Ostrow, L. W.; Baas, F.; Zaitlen, N.; Berry, J. D.; Malaspina, A.; Fratta, P.; Cox, G. A.; Thompson, L. M.; Finkbeiner, S.; Dardiotis, E.; Miller, T. M.; Chandran, S.; Pal, S.; Hornstein, E.; MacGowan, D. J.; Heiman-Patterson, T.; Hammell, M. G.; Patsopoulos, N. A.; Butovsky, O.; Dubnau, J.; Nath, A.; Bowser, R.; Harms, M.; Poss, M.; Phillips-Cremins, J.; Crary, J.; Atassi, N.; Lange, D. J.; Adams, D. J.; Stefanis, L.; Gotkine, M.; Baloh, R. H.; Babu, S.; Raj, T.; Paganoni, S.; Shalem, O.; Smith, C.; Zhang, B.; Harris, B.; Broce, I.; Drory, V.; Ravits, J.; McMillan, C.; Menon, V.; Wu, L.; Altschuler, S. An Integrated Multi-Omic Analysis of iPSC-Derived Motor Neurons from C9ORF72 ALS Patients. *iScience* **2021**, *24* (11), n/a.

(10) Pang, Z.; Chong, J.; Zhou, G.; De Lima Morais, D. A.; Chang, L.; Barrette, M.; Gauthier, C.; Jacques, P. É.; Li, S.; Xia, J. MetaboAnalyst 5.0: Narrowing the Gap between Raw Spectra and Functional Insights. *Nucleic Acids Res.* **2021**, *49* (W1), W388−W396.

(11) Li, F.; Song, J.; Zhang, Y.; Wang, S.; Wang, J.; Lin, L.; Yang, C.; Li, P.; Huang, H. LINT-Web: A Web-Based Lipidomic Data Mining Tool Using Intra-Omic Integrative Correlation Strategy. *Small Methods* **2021**, *5* (9), n/a.

(12) Athieniti, E.; Spyrou, G. M. A Guide to Multi-Omics Data Collection and Integration for Translational Medicine. *Comput. Struct Biotechnol J.* **2023**, *21*, 134−149.

(13) Dickinson, Q.; Kohler, A.; Ott, M.; Meyer, J. G Multi-Omic Integration by Machine Learning (MIMaL). *Bioinformatics* **2022**, *38* (21), 4908−4918.

(14) Zhao, N.; Quicksall, Z.; Asmann, Y. W.; Ren, Y. Network Approaches for Omics Studies of Neurodegenerative Diseases. *Front Genet* **2022**, *13*, No. 984338.

(15) Kao, A. W.; McKay, A.; Singh, P. P.; Brunet, A.; Huang, E. J. Progranulin, Lysosomal Regulation and Neurodegenerative Disease. *Nat. Rev. Neurosci* **2017**, *18* (6), 325−333.

(16) Petkau, T. L.; Leavitt, B. R. Progranulin in Neurodegenerative Disease. *Trends Neurosci* **2014**, *37* (7), 388−398.

(17) Tolkatchev, D.; Malik, S.; Vinogradova, A.; Wang, P.; Chen, Z.; Xu, P.; Bennett, H. P. J.; Bateman, A.; Ni, F. Structure Dissection of Human Progranulin Identifies Well-folded Granulin/Epithelin Modules with Unique Functional Activities. *Protein Sci.* **2008**, *17* (4), 711−724.

(18) Paushter, D. H.; Du, H.; Feng, T.; Hu, F. The Lysosomal Function of Progranulin, a Guardian against Neurodegeneration. *Acta Neuropathol* **2018**, *136* (1), 1−17.

(19) Chang, M. C.; Srinivasan, K.; Friedman, B. A.; Suto, E.; Modrusan, Z.; Lee, W. P.; Kaminker, J. S.; Hansen, D. V.; Sheng, M. Progranulin Deficiency Causes Impairment of Autophagy and TDP-43 Accumulation. *Journal of Experimental Medicine* **2017**, *214* (9), 2611−2628.

(20) Gao, X.; Joselin, A. P.; Wang, L.; Kar, A.; Ray, P.; Bateman, A.; Goate, A. M.; Wu, J. Y. Progranulin Promotes Neurite Outgrowth and Neuronal Differentiation by Regulating GSK-3β. *Protein Cell* **2010**, *1*, 552.

(21) Boland, S.; Swarup, S.; Ambaw, Y. A.; Malia, P. C.; Richards, R. C.; Fischer, A. W.; Singh, S.; Aggarwal, G.; Spina, S.; Nana, A. L.; Grinberg, L. T.; Seeley, W. W.; Surma, M. A.; Klose, C.; Paulo, J. A.; Nguyen, A. D.; Harper, J. W.; Walther, T. C.; Farese, R. V. Deficiency of the Frontotemporal Dementia Gene GRN Results in Gangliosidosis. *Nat. Commun.* **2022**, *13* (1), n/a.

(22) Hasan, S.; Fernandopulle, M. S.; Humble, S. W.; Frankenfield, A. M.; Li, H.; Prestil, R.; Johnson, K. R.; Ryan, B. J.; Wade-Martins, R.; Ward, M. E.; Hao, L. Multi-Modal Proteomic Characterization of Lysosomal Function and Proteostasis in Progranulin-Deficient Neurons. *Mol. Neurodegener* **2023**, *18* (1), 87.

https://doi.org/10.1021/acs.jproteome.3c00790
J. Proteome Res. XXXX, XXX, XXX−XXX

(23) Wang, C.; Ward, M. E.; Chen, R.; Liu, K.; Tracy, T. E.; Chen, X.; Xie, M.; Sohn, P. D.; Ludwig, C.; Meyer-Franke, A.; Karch, C. M.; Ding, S.; Gan, L. Scalable Production of iPSC-Derived Human Neurons to Identify Tau-Lowering Compounds by High-Content Screening. *Stem Cell Reports* **2017**, *9* (4), 1221−1233.
(24) Frankenfield, A. M.; Fernandopulle, M. S.; Hasan, S.; Ward, M. E.; Hao, L. Development and Comparative Evaluation of Endolysosomal Proximity Labeling-Based Proteomic Methods in Human iPSC-Derived Neurons. *Anal. Chem.* **2020**, *92* (23), 15437−15444.
(25) Folch, J.; Lees, M.; Stanley, G. H. S. A SIMPLE METHOD FOR THE ISOLATION AND PURIFICATION OF TOTAL LIPIDES FROM ANIMAL TISSUES*. *J. Biol. Chem.* **1957**, *226* (1), 497−509.
(26) Frankenfield, A. M.; Ni, J.; Ahmed, M.; Hao, L. Protein Contaminants Matter: Building Universal Protein Contaminant Libraries for DDA and DIA Proteomics. *J. Proteome Res.* **2022**, *21* (9), 2104−2113.
(27) Koelmel, J. P.; Kroeger, N. M.; Ulmer, C. Z.; Bowden, J. A.; Patterson, R. E.; Cochran, J. A.; Beecher, C. W. W.; Garrett, T. J.; Yost, R. A. LipidMatch: An Automated Workflow for Rule-Based Lipid Identification Using Untargeted High-Resolution Tandem Mass Spectrometry Data. *BMC Bioinformatics* **2017**, *18* (1), n/a.
(28) Dei Cas, M.; Zulueta, A.; Mingione, A.; Caretti, A.; Ghidoni, R.; Signorelli, P.; Paroni, R. An Innovative Lipidomic Workflow to Investigate the Lipid Profile in a Cystic Fibrosis Cell Line. *Cells* **2020**, *9* (5), 1197.
(29) Li, H.; Uittenbogaard, M.; Navarro, R.; Ahmed, M.; Gropman, A.; Chiaramello, A.; Hao, L. Integrated Proteomic and Metabolomic Analyses of the Mitochondrial Neurodegenerative Disease MELAS. *Mol. Omics* **2022**, *18* (3), 196−205.
(30) Hao, L.; Greer, T.; Page, D.; Shi, Y.; Vezina, C. M.; Macoska, J. A.; Marker, P. C.; Bjorling, D. E.; Bushman, W.; Ricke, W. A.; Li, L. In-Depth Characterization and Validation of Human Urine Metabolomes Reveal Novel Metabolic Signatures of Lower Urinary Tract Symptoms. *Sci. Rep* **2016**, *6*, No. 30869.
(31) MacLean, B.; Tomazela, D. M.; Shulman, N.; Chambers, M.; Finney, G. L.; Frewen, B.; Kern, R.; Tabb, D. L.; Liebler, D. C.; MacCoss, M. J. Skyline: An Open Source Document Editor for Creating and Analyzing Targeted Proteomics Experiments. *Bioinformatics* **2010**, *26* (7), 966−968.
(32) Goedhart, J.; Luijsterburg, M. S. VolcaNoseR Is a Web App for Creating, Exploring, Labeling and Sharing Volcano Plots. *Sci. Rep* **2020**, *10* (1), n/a.
(33) Ge, S. X.; Jung, D.; Yao, R. ShinyGO: A Graphical Gene-Set Enrichment Tool for Animals and Plants. *Bioinformatics* **2020**, *36* (8), 2628−2629.
(34) Molenaar, M. R.; Jeucken, A.; Wassenaar, T. A.; Van De Lest, C. H. A.; Brouwers, J. F.; Helms, J. B. LION/Web: A Web-Based Ontology Enrichment Tool for Lipidomic Data Analysis. *Gigascience* **2019**, *8* (6), n/a.
(35) Lopez-Ibanez, J.; Pazos, F.; Chagoyen, M. MBROLE3: Improved Functional Enrichment of Chemical Compounds for Metabolomics Data Analysis. *Nucleic Acids Res.* **2023**, *51* (W1), W305−W309.
(36) Ramos, A.; Camargo, F. D. The Hippo Signaling Pathway and Stem Cell Biology. *Trends Cell Biol.* **2012**, *22* (7), 339−346.
(37) Söhl, G.; Maxeiner, S.; Willecke, K. Expression and Functions of Neuronal Gap Junctions. *Nat. Rev. Neurosci* **2005**, *6* (3), 191−200.
(38) Hosseini, V.; Kalantary-Charvadeh, A.; Hajikarami, M.; Fayyazpour, P.; Rahbarghazi, R.; Totonchi, M.; Darabi, M. A Small Molecule Modulating Monounsaturated Fatty Acids and Wnt Signaling Confers Maintenance to Induced Pluripotent Stem Cells against Endodermal Differentiation. *Stem Cell Res. Ther* **2021**, *12* (1), n/a.
(39) Liang, Y. J.; Kuo, H. H.; Lin, C. H.; Chen, Y. Y.; Yang, B. C.; Cheng, Y. Y.; Yu, A. L.; Khoo, K. H.; Yu, J. Switching of the Core Structures of Glycosphingolipids from Globo- and Lacto- to Ganglio-Series upon Human Embryonic Stem Cell Differentiation. *Proc. Natl. Acad. Sci. U. S. A.* **2010**, *107* (52), 22564−22569.
(40) Janssen, C. I. F.; Kiliaan, A. J. Long-Chain Polyunsaturated Fatty Acids (LCPUFA) from Genesis to Senescence: The Influence of LCPUFA on Neural Development, Aging, and Neurodegeneration. *Prog. Lipid Res.* **2014**, *53* (1), 1−17.
(41) Tsai, Y. T.; Itokazu, Y.; Yu, R. K. GM1 Ganglioside Is Involved in Epigenetic Activation Loci of Neuronal Cells. *Neurochem. Res.* **2016**, *41* (1−2), 107−115.
(42) Falabella, M.; Vernon, H. J.; Hanna, M. G.; Claypool, S. M.; Pitceathly, R. D. S. Cardiolipin, Mitochondria, and Neurological Disease. *Trends in Endocrinology and Metabolism* **2021**, *32* (4), 224−237.
(43) Kagan, T.; Stoyanova, G.; Lockshin, R. A.; Zakeri, Z. Ceramide from Sphingomyelin Hydrolysis Induces Neuronal Differentiation, Whereas de Novo Ceramide Synthesis and Sphingomyelin Hydrolysis Initiate Apoptosis after NGF Withdrawal in PC12 Cells. *Cell Communication and Signaling* **2022**, *20* (1), n/a.
(44) Keilhoff, G.; Mbou, R. P.; Lucas, B.; Schild, L. The Differentiation of Spinal Cord Motor Neurons Is Associated with Changes of the Mitochondrial Phospholipid Cardiolipin. *Neuroscience* **2019**, *400*, 169−183.
(45) Yoon, J. H.; Seo, Y.; Jo, Y. S.; Lee, S.; Cho, E.; Cazenave-Gassiot, A.; Shin, Y.-S.; Moon, M. H.; An, H. J.; Wenk, M. R.; Suh, P.-G. Brain Lipidomics: From Functional Landscape to Clinical Significance. *Sci. Adv.* **2022**, *8*, 9317.
(46) Lin, T.; Islam, O.; Heese, K. ABC Transporters, Neural Stem Cells and Neurogenesis - A Different Perspective. *Cell Res.* **2006**, *16* (11), 857−871.
(47) Rigaud, V. O. C.; Hoy, R.; Mohsin, S.; Khan, M. Stem Cell Metabolism: Powering Cell-Based Therapeutics. *Cells* **2020**, *9* (11), 2490.
(48) Südhof, T. C. The Synaptic Vesicle Cycle. *Annu. Rev. Neurosci.* **2004**, *27*, 509−547.
(49) Picciotto, M. R.; Higley, M. J.; Mineur, Y. S. Acetylcholine as a Neuromodulator: Cholinergic Signaling Shapes Nervous System Function and Behavior. *Neuron* **2012**, *76* (1), 116−129.
(50) Carsana, E. V.; Audano, M.; Breviario, S.; Pedretti, S.; Aureli, M.; Lunghi, G.; Mitro, N. Metabolic Profile Variations along the Differentiation of Human-Induced Pluripotent Stem Cells to Dopaminergic Neurons. *Biomedicines* **2022**, *10* (9), 2069.
(51) Gass, J.; Lee, W. C.; Cook, C.; Finch, N.; Stetler, C.; Jansen-West, K.; Lewis, J.; Link, C. D.; Rademakers, R.; Nykjær, A.; Petrucelli, L. Progranulin Regulates Neuronal Outgrowth Independent of Sortilin. *Mol. Neurodegener* **2012**, *7* (1), n/a.
(52) Evers, B. M.; Rodriguez-Navas, C.; Tesla, R. J.; Prange-Kiel, J.; Wasser, C. R.; Yoo, K. S.; McDonald, J.; Cenik, B.; Ravenscroft, T. A.; Plattner, F.; Rademakers, R.; Yu, G.; White, C. L.; Herz, J. Lipidomic and Transcriptomic Basis of Lysosomal Dysfunction in Progranulin Deficiency. *Cell Rep* **2017**, *20* (11), 2565−2574.
(53) Aflaki, E.; Radović, B.; Chandak, P. G.; Kolb, D.; Eisenberg, T.; Ring, J.; Fertschai, I.; Uellen, A.; Wolinski, H.; Kohlwein, S. D.; Zechner, R.; Levak-Frank, S.; Sattler, W.; Graier, W. F.; Malli, R.; Madeo, F.; Kratky, D. Triacylglycerol Accumulation Activates the Mitochondrial Apoptosis Pathway in Macrophages. *J. Biol. Chem.* **2011**, *286* (9), 7418−7428.
(54) Chatterjee, S.; Balram, A.; Li, W. Convergence: Lactosylceramide-Centric Signaling Pathways Induce Inflammation, Oxidative Stress, and Other Phenotypic Outcomes. *Int. J. Mol. Sci.* **2021**, *22* (4), 1−25.
(55) Hannun, Y. A.; Obeid, L. M. Sphingolipids and Their Metabolism in Physiology and Disease. *Nat. Rev. Mol. Cell Biol.* **2018**, *19* (3), 175−191.
(56) Stith, J. L.; Velazquez, F. N.; Obeid, L. M. Advances in Determining Signaling Mechanisms of Ceramide and Role in Disease. *J. Lipid Res.* **2019**, *60* (5), 913−918.
(57) Dorninger, F.; Forss-Petter, S.; Berger, J. From Peroxisomal Disorders to Common Neurodegenerative Diseases − the Role of

https://doi.org/10.1021/acs.jproteome.3c00790
J. Proteome Res. XXXX, XXX, XXX−XXX

Ether Phospholipids in the Nervous System. *FEBS Lett.* **2017**, *591* (18), 2761−2788.
(58) Mulder, C.; Wahlund, L. O.; Teerlink, T.; Blomberg, M.; Veerhuis, R.; Van Kamp, G. J.; Scheltens, P.; Scheffer, P. G. Decreased Lysophosphatidylcholine/Phosphatidylcholine Ratio in Cerebrospinal Fluid in Alzheimer's Disease. *J. Neural Transm* **2003**, *110* (8), 949−955.
(59) Cooper, A. J. L. ROLE OF GLUTAMINE IN CEREBRAL NITROGEN METABOLISM AND AMMONIA NEUROTOXICITY. *Ment Retard Dev Disabil Res. Rev.* **2001**, *7*, 280−286.
(60) Kaur, G.; Rathod, S. S. S.; Ghoneim, M. M.; Alshehri, S.; Ahmad, J.; Mishra, A.; Alhakamy, N. A. DNA Methylation: A Promising Approach in Management of Alzheimer's Disease and Other Neurodegenerative Disorders. *Biology (Basel)* **2022**, *11* (1), 90.
(61) Martínez-Reyes, I.; Chandel, N. S. Mitochondrial TCA Cycle Metabolites Control Physiology and Disease. *Nat. Commun.* **2020**, *11* (1), n/a.
(62) Cui, C.; Sun, J.; Pawitan, Y.; Piehl, F.; Chen, H.; Ingre, C.; Wirdefeldt, K.; Evans, M.; Andersson, J.; Carrero, J. J.; Fang, F. Creatinine and C-Reactive Protein in Amyotrophic Lateral Sclerosis, Multiple Sclerosis and Parkinson's Disease. *Brain Commun.* **2020**, *2* (2), n/a.
(63) Micheli, V.; Camici, M.; Tozzi, M. G.; Ipata, P. L.; Sestini, S.; Bertelli, M.; Pompucci, G. Neurological Disorders of Purine and Pyrimidine Metabolism. *Curr. Top Med. Chem.* **2011**, *11*, 923−947.
(64) Cansev, M. Uridine and Cytidine in the Brain: Their Transport and Utilization. *Brain Res. Rev.* **2006**, *52* (2), 389−397.
(65) Shirai, Y.; Kouzuki, T.; Kakefuda, K.; Moriguchi, S.; Oyagi, A.; Horie, K.; Morita, S. Y.; Shimazawa, M.; Fukunaga, K.; Takeda, J.; Saito, N.; Hara, H. Essential Role of Neuron-Enriched Diacylglycerol Kinase (DGK), DGKβ in Neurite Spine Formation, Contributing to Cognitive Function. *PLoS One* **2010**, *5* (7), n/a.
(66) Singh, M. Neuroprotection: Pharmacological Approaches. *Encyclopedia of Neuroscience* **2009**, 967−970.
(67) Ferrucci, A.; Nonnemacher, M. R.; Wigdahl, B. Human Immunodeficiency Virus Viral Protein R as an Extracellular Protein in Neuropathogenesis. In *Advances in Virus Research*; Academic Press Inc., 2011; Vol. *81*, pp 165−199. DOI: 10.1016/B978-0-12-385885-6.00010-9.
(68) Woo, M. S.; Ufer, F.; Rothammer, N.; Di Liberto, G.; Binkle, L.; Haferkamp, U.; Sonner, J. K.; Engler, J. B.; Hornig, S.; Bauer, S.; Wagner, I.; Egervari, K.; Raber, J.; Duvoisin, R. M.; Pless, O.; Merkler, D.; Friese, M. A. Neuronal Metabotropic Glutamate Receptor 8 Protects against Neurodegeneration in CNS Inflammation. *Journal of Experimental Medicine* **2021**, *218* (5), n/a.
(69) Menniti, F. S.; Faraci, W. S.; Schmidt, C. J. Phosphodiesterases in the CNS: Targets for Drug Development. *Nat. Rev. Drug Discovery* **2006**, *5* (8), 660−670.

https://doi.org/10.1021/acs.jproteome.3c00790
J. Proteome Res. XXXX, XXX, XXX−XXX